

REACT: Real-time Entanglement-Aware Coverage Path Planning for Tethered Underwater Vehicles

Abdelhakim Amer, Mohit Mehndratta, Yury Brodskiy, Bilal Wehbe and Erdal Kayacan

Abstract—Inspection of complex underwater structures with tethered underwater vehicles is often hindered by the risk of tether entanglement. We propose REACT (real-time entanglement-aware coverage path planning for tethered underwater vehicles), a framework designed to overcome this limitation. REACT comprises a fast geometry-based tether model using the signed distance field (SDF) map for accurate, real-time simulation of taut tether configurations around arbitrary structures in 3D. This model enables an efficient online replanning strategy by enforcing a maximum tether length constraint, thereby actively preventing entanglement. By integrating REACT into a coverage path planning framework, we achieve safe and optimal inspection paths, previously challenging due to tether constraints. The complete REACT framework’s efficacy is validated in a pipe inspection scenario, demonstrating safe, entanglement-free navigation and full-coverage inspection. Simulation results show that REACT achieves complete coverage while maintaining tether constraints and completing the total mission 20% faster than conventional planners, despite a longer inspection time due to proactive avoidance of entanglement that eliminates extensive post-mission disentangling. Real-world experiments confirm these benefits, where REACT completes the full mission, while the baseline planner fails due to physical tether entanglement.

I. INTRODUCTION

Operating in complex, hazardous, and otherwise inaccessible environments, remotely operated vehicles (ROVs) have become essential for modern exploration and intervention tasks. They enable a diverse range of demanding applications, including surveying, infrastructure inspection, and deep-sea exploration [1]–[3], thereby expanding operational possibilities. Most ROVs are tethered to a host platform to maintain reliable communication and ensure a continuous power supply during long-duration missions. However, this tethering infrastructure introduces operational challenges related to planning and control while posing the risk of being entangled with underwater objects such as flora, fauna, or underwater structures.

Numerous coverage path planner (CPP) algorithms are proposed in the literature for inspection-related tasks with un-

A. Amer is with the Artificial Intelligence in Robotics Laboratory (AiR Lab), Department of Electrical and Computer Engineering, Aarhus University, 8000 Aarhus C, Denmark {abdelhakim} at ece.au.dk. Mohit Mehndratta is with GIM Robotics, Espoo, Finland, {mohit.mehndiratta} at gimrobotics.fi. Y. Brodskiy is with EIVA a/s, 8660 Skanderborg, Denmark. {ybr} at eiva.com. B. Wehbe is with Deutsches Forschungszentrum für Künstliche Intelligenz GmbH (DFKI), Bremen, Germany. {bilal.wehbe} at dfki.de. E. Kayacan is with the Automatic Control Group, Department of Electrical Engineering and Information Technology, Paderborn University, Paderborn, Germany. {erdal.kayacan} at uni-paderborn.de.

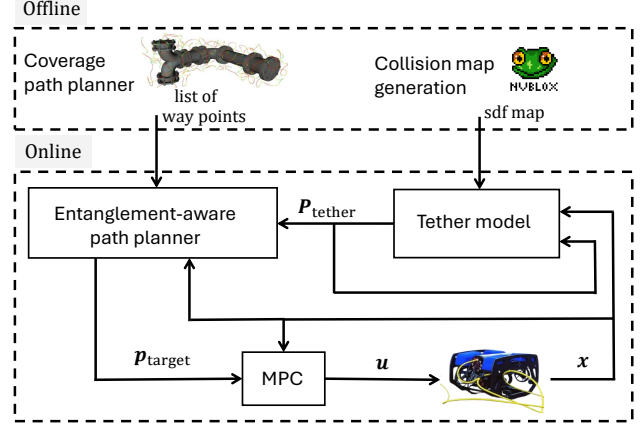


Fig. 1: Overview of the real-time entanglement-aware coverage path planning for tethered underwater vehicles (REACT) inspection framework. Offline, a signed distance field (SDF) map is generated from a point cloud, and an off-the-shelf CPP [8] is used to compute an optimal waypoint sequence. During operation, a tether model (P_{tether}) is used to ensure tether length is not exceeded, while a model predictive control (MPC) applies the optimal wrench u to the ROV.

tethered systems [4]–[6]. In essence, they compute distance-optimal paths for a thorough inspection of 3D structures [7]–[9]. Additionally, exploration path planners are employed to determine the next viewpoints for mapping unknown terrains [10], [11]. However, these path-planning methods are restricted to untethered systems, as they do not account for possible entanglements with the surroundings. Hence, the literature still lacks path-planning algorithms that directly address tether-related challenges.

During operation, entanglement can occur when the vehicle’s movement is restricted due to interaction between the tether and objects in the environment. The tether can loop around obstacles, thereby limiting the vehicle’s mobility and substantially reducing operational range in a worst-case scenario. Consequently, operators need to carry longer tethers to account for possible entanglements without a proper planner at hand. In this work, we propose REACT that fills this gap in underwater asset inspection. In essence, when integrated into the coverage path planning framework, REACT renders entanglement-free paths, thus ensuring task completion without the need to carry additional tether lengths. Besides, the proposed planning framework reduces overall operational time by circumventing the post-completion detangling process, often required with traditional path-planning methods.

The contributions of this work can be summarized as follows:

- A computationally efficient tether model that computes the tether configuration using the SDF map of arbitrary underwater structures.
- An efficient online replanning method that prevents entanglement by incorporating a tether-length constraint.
- Integration with an off-the-shelf CPP along with MPC, rendering optimal inspection trajectory.
- Demonstration of the framework in simulation and real-world tests, showcasing its ability to ensure safe and time-efficient inspection.

The remainder of this paper is organized as follows: Section II reviews related work. Section III presents the overall framework for tethered underwater inspection. Section IV introduces the taut-tether model, and Section V describes the proposed planner. Experimental results are shown in Sections VI and VII, followed by conclusions in Section VIII.

II. STATE OF THE ART

The risk of entanglement with obstacles presents a serious challenge for robots with conventional path planners. To systematically address this, a taxonomy of entanglement definitions was presented in [12], where existing interpretations from the literature were cataloged and new definitions were introduced, paving the way for developing new path planning strategies that account for entanglement.

Initial efforts to develop entanglement-aware path planners were often focused on two-dimensional environments and employed offline computation strategies. For instance, in [13] and [14], methods were proposed for planning paths in 2D to cover a predefined set of waypoints while considering tether constraints. Notably, in [14], the path planning problem for a ROV was formulated as a mixed-integer programming problem. In that approach, a traveling salesman problem (TSP) was first solved to find an optimal waypoint sequence, and then homotopic constraints were incorporated during path generation to minimize the likelihood of tether entanglement. While effective for predefined scenarios, these offline methods lack the adaptability required for dynamic environments. A more recent approach to the 2D coverage path planning problem for tethered robots was presented in [15], where spanning tree-based offline optimization was employed.

To address the need for real-time adaptability, subsequent research explored online path planning algorithms, still primarily in 2D. In [16], a homotopy-augmented topological approach combined with graph search techniques was introduced, allowing for dynamic adjustments to the path based on environmental perception. Similarly, in [17], a hybrid A* variant utilizing a modified tangent graph was developed. This method efficiently plans curvature-constrained paths for tethered robots subject to winding angle constraints, demonstrating guarantees and providing simulation results for online entanglement avoidance.

The complexity of tether management increases significantly when coordinating multiple robots. Foundational work

in this area was laid in [18], followed by methods proposed in [19]. More recently, in [20], an efficient online path planner for multi-robot systems was presented. In this method, a homotopy-based high-level planner was integrated with trajectory optimization and smoothing techniques to generate entanglement-free paths. However, despite its online capability, this approach remains constrained to 2D environments.

The online planners described above represent a significant step towards real-time tether management; however, they are limited to 2D environments. Moreover, while preventive paths to avoid entanglement can be planned, strategies for path planning once tether entanglement has already occurred are not provided.

Real-world applications frequently require navigation in 3D environments, such as with underwater robots. Consequently, in [21] and [22], topological aspects and optimization techniques for 3D tethered navigation were explored. In [23], a 3D exploration path planner incorporating explicit contact avoidance constraints for the tether was presented, facilitating safer navigation for single tethered robots in complex three-dimensional spaces.

The increased complexity of 3D multi-robot scenarios was addressed in [24], where earlier 2D work was extended to three dimensions. Further advancements were introduced in [25] and [26], where path planning strategies explicitly considering the topological constraints imposed by multiple interacting tethers in 3D were proposed. While these methods advance the state of the art in multi-robot coordination, they are generally designed for offline computation and are not suited for online path planning where real-time implementation is essential.

In summary, existing path planners that account for tether constraints often face limitations for practical online CPP in complex 3D settings. Many are too computationally intensive for real-time use [14], [24]–[26], lack integrated tether-aware CPP frameworks, or rely on simplifying assumptions such as 2D environments or basic obstacle shapes [16], [17], [20], hindering generalization to real-world inspection tasks.

To address these limitations, a novel approach named REACT is proposed, which enables real-time, entanglement-aware path planning in arbitrary 3D environments.

III. OVERALL REACT FRAMEWORK

REACT framework, as depicted in Fig. 1, consists of two main components: an offline planning phase and an online execution phase. In the offline phase, the environment is provided as a point cloud, including the object to be inspected. Then, a SDF map is generated from this point cloud using the nvblox library [27]. Subsequently, the extracted point cloud of the structure under inspection is processed via FC-Planner [8] to compute an optimal waypoint sequence, generating a path that renders full inspection coverage while disregarding the tether constraints.

In the online phase, tether constraints are handled by an entanglement-aware replanner that ensures that the maximum tether length is not exceeded due to entanglement. This is achieved using our developed tether model, which continuously updates based on the current state of the tether and the

new position of the ROV, denoted as \mathbf{p}_{rov} . The online planner then provides the reference state to an MPC controller, which computes and applies the optimal wrench to the ROV.

IV. TETHER MODELING

In this section, we describe a computationally efficient, geometry-based tether model for tethered underwater vehicles. This model predicts the tether path, specifically the positions of each node along the tether's length, based on the ROV's trajectory, and assumes a geometry-based constraint where the tether remains taut and fully stretched at all times. The main idea of the proposed tether model is inspired by the shortcutting algorithm of the ropeRRT path planner [28], which simplifies sampled trajectories similar to a rope tightening around an obstacle.

A. Tether model description

Let the tether path at time t be denoted by $\mathbf{P}_{\text{tether}}(t) = \{\mathbf{p}_i(t)\}_{i=1}^n$, where each node $\mathbf{p}_i(t) \in \mathbb{R}^3$ represents the position of the i -th node in 3D space at time t , and n is the total number of nodes in the tether path. The ROV position at time t , denoted by $\mathbf{p}_{\text{rov}}(t) \in \mathbb{R}^3$, is appended at the end $\mathbf{p}_{n+1}(t)$, ensuring that the ROV's position is included in the tether path.

The proposed tether model then iteratively computes the equivalent taut-tether path through sequential shortcutting operation. Fig. 2 illustrates an example of the shortcut operation. Starting at the last node ($\mathbf{p}_j(t) = \mathbf{p}_n(t)$), the algorithm attempts to shortcut the path segment between each pair of nodes ($\mathbf{p}_i(t), \mathbf{p}_j(t)$) where $i > j$. If the line of sight between $\mathbf{p}_i(t)$ and $\mathbf{p}_j(t)$ is collision-free, as determined via an SDF map (\mathcal{M}_{sdf}), the intermediate nodes are replaced with a straight segment sampled at known resolution δ . Conversely, if the line of sight encounters a collision, j shifts to the preceding node, and the collision-free line of sight is rechecked. This process is repeated until a collision-free line of sight is found, and the intermediate nodes are then replaced.

Finally, after the shortcutting step, a pulling operation is applied to each node, moving it incrementally toward the tether endpoint $\mathbf{p}_{n+1}(t)$. This ensures that nodes are not left stuck in the cavities of non-convex obstacles. The shortcutting and pulling operations are applied iteratively until convergence, resulting in a taut and collision-free tether path $\mathbf{P}_{\text{tether}}(t+1)$. The full procedure is described in Algorithm 1.

V. ENTANGLEMENT-AWARE PATH PLANNER

Next, we present the entanglement-aware path planner, a local planner designed to address the real-time entanglement avoidance problem for tethered underwater vehicles. The planner continuously monitors the tether configuration and dynamically adjusts the vehicle's target to prevent the tether length from exceeding a specified maximum allowable length, L_{max} , while ensuring safe navigation toward a series of predefined reference waypoints.

Algorithm 1: Taut-tether model

Input : $\mathbf{p}_{\text{rov}}(t), \mathbf{P}_{\text{tether}}(t), \mathcal{M}_{\text{sdf}}, \delta$
Return: $\mathbf{P}_{\text{tether}}(t+1)$

```

appendPath( $\mathbf{P}_{\text{tether}}(t), \mathbf{p}_{\text{rov}}(t)$ );
for  $i \leftarrow \text{len}(\mathbf{P}_{\text{tether}}(t)) - 1$  to 0 do
    for  $j \leftarrow i - 1$  to 0 do
        if checkShortcut( $\mathbf{P}_{\text{tether}}(t), i, j$ ) then
            replaceNodes( $\mathbf{P}_{\text{tether}}(t), i, j, \delta$ );
        else
            if not checkLineOfSight ( $\mathcal{M}_{\text{sdf}},$ 
                 $\mathbf{P}_{\text{tether}}(t)$ ) then
                break;
            if isInCollision( $\mathcal{M}_{\text{sdf}}, \mathbf{P}_{\text{tether}}(t)[j]$ ) then
                pullNode( $\mathbf{P}_{\text{tether}}(t)[j],$ 
                     $\mathbf{P}_{\text{tether}}(t).\text{end}(), \delta$ );
    return  $\mathbf{P}_{\text{tether}}(t+1)$ ;

```

At each time step t , the planner receives the current estimated tether path, $\mathbf{P}_{\text{tether}}(t)$, from the tether model. It also maintains an ordered list of target waypoints, $\mathbf{W} = \{\mathbf{p}_{\text{waypoint}}(k)\}_{k=1}^m$, where each $\mathbf{p}_{\text{waypoint}}(k)$ specifies a 3D position the ROV must reach sequentially. The current position of the ROV, $\mathbf{p}_{\text{rov}}(t)$, and the current waypoint index, k , are also maintained as part of the planner's state.

The current tether length $L_{\text{tether}}(t)$ is computed from the tether path and compared against the maximum allowable tether length L_{max} to determine whether re-planning is necessary.

The planner operates in two main modes: normal mode and recovery mode. In normal mode, when the tether length is within the allowable limit, the planner sets the ROV's target position directly to the current waypoint. It continuously monitors the ROV's position and, upon detecting that the waypoint has been reached, advances the waypoint index to the next target in the sequence. This mode prioritizes nominal waypoint following behavior.

If the tether length exceeds the limit, the planner switches to recovery mode to avoid entanglement. In this mode, a recovery path is generated by searching for an alternative safe path toward the current waypoint that respects the tether length constraint. The ROV's target position, $\mathbf{p}_{\text{target}}$, is then updated to incrementally follow this recovery path. The planner remains in recovery mode until the end of the recovery path is reached, at which point it switches back to normal mode to continue waypoint tracking.

This dual-mode approach ensures that the vehicle maintains a safe tether configuration while effectively progressing through its mission waypoints. By continuously switching between nominal waypoint tracking and recovery behaviors in response to tether length measurements, the planner enables real-time, entanglement-aware path planning. The overall entanglement-aware planning framework is summarized in Algorithm 2.

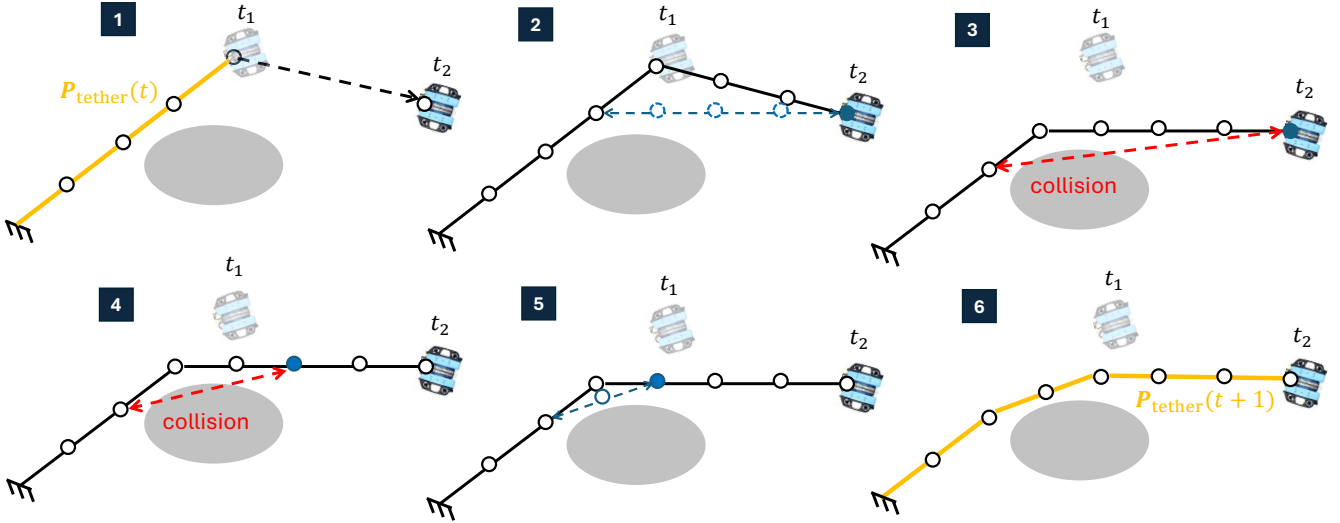


Fig. 2: Tether shortcutting during ROV motion from t_1 to t_2 . (1) Initial tether with new ROV position \mathbf{p}_{rov} appended; (2) Successful shortcut from the end node; (3) Collision encountered when attempting further shortcutting, skipping to the next node; (4) Another collision detected from the new node; (5) Successful shortcut from a subsequent node; (6) Final tether configuration (yellow) after applying all feasible shortcuts.

A. Disentanglement path search

To implement the disentanglement behavior described above, the recovery path search algorithm (Algorithm 3) is employed. This algorithm takes as input the current tether path $\mathbf{P}_{\text{tether}}(t)$, the current target waypoint $\mathbf{W}[k]$, and the maximum allowable tether length L_{max} . Its goal is to generate a recovery path $\mathbf{P}_{\text{recovery}}$ that guides the ROV safely toward the waypoint while ensuring that the tether length constraint is respected.

The algorithm performs a backward search along the tether path, starting from the ROV's current position at the tether's end and progressing toward toward the tether starting node (\mathbf{p}_0). At each iteration, a candidate pivot point $\mathbf{p}_{\text{pivot}}$ on the tether is selected as a potential point from which the ROV can attempt an alternative route toward the target waypoint.

For each pivot, two path segments are constructed. The first segment, \mathbf{P}_{r1} , corresponds to the reversed portion of the tether from the pivot $\mathbf{p}_{\text{pivot}}$ to the ROV's current position, representing the retraced section of the tether. The second segment, $\mathbf{P}_{s(n-i)}$, is a newly planned shortest path connecting the pivot to the target waypoint $\mathbf{W}[k]$, which can be computed using sampling-based methods such as RRT*. These segments are then concatenated with the tether path from \mathbf{p}_0 up to the pivot, forming an augmented candidate path \mathbf{P}_{aug} .

This candidate path \mathbf{P}_{aug} is used to simulate the tether configuration and estimate its length L_{tether} at the next time step. The total tether length L_{tether} is then compared against the maximum allowable length L_{max} . If the length constraint is satisfied, the recovery path $\mathbf{P}_{\text{recovery}} = \mathbf{P}_{r1} \cup \mathbf{P}_{s(n-i)}$ is considered feasible and returned.

If no feasible path is found after examining all possible pivot points, the algorithm defaults to a fallback strategy where the tether length constraint is treated as a soft limit.

In this case, the recovery path consists solely of the shortest path from the ROV's current position directly to the target waypoint, temporarily disregarding tether length constraints.

The resulting recovery path provides a safe and viable trajectory for the ROV to follow during disentanglement operations by combining the reversed tether segment (if applicable) with the newly planned path toward the waypoint, as illustrated in Figure 3.

B. Recovery path refinement

The initially selected recovery path $\mathbf{P}_{\text{recovery}}$ undergoes further refinement to enhance safety and smoothness before execution. This involves three steps:

- 1) Centroid Offsetting: Points along $\mathbf{P}_{\text{recovery}}$ are pushed slightly outwards, away from the path's geometric centroid, to increase clearance from potential obstacles near the path's center.
- 2) Random Sampling Perturbation: Points are locally perturbed by sampling in random directions, seeking nearby collision-free states to potentially escape minor constraint violations or local minima.
- 3) Polynomial Smoothing: A third order polynomial function is fitted to segments of the path to reduce sharp turns and generate a smoother reference trajectory.

The planner then checks if $\mathbf{P}_{\text{recovery}}$ is collision-free. This refinement process is performed in a loop that continues until a collision-free path is found.

VI. SIMULATIONS EXPERIMENTS

This section presents the simulation results for the proposed REACT method. The entire framework is implemented in C++ to ensure computational efficiency and is integrated with ROS to facilitate modularity and deployment on real-world robots. Furthermore, the open motion planning

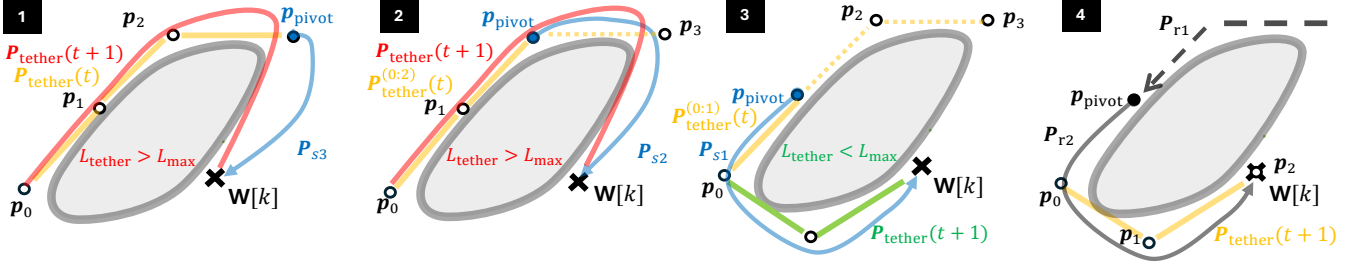


Fig. 3: Disentanglement path search process. At time t , the tether configuration is $\mathbf{P}_{\text{tether}}(t) = \{p_0, p_1, p_2, p_3\}$. (1) The shortest path \mathbf{P}_{s3} from p_3 to the waypoint $\mathbf{W}[k]$ is appended to the tether path, forming the augmented path $\mathbf{P}_{\text{tether}}^{(0:3)} \cup \mathbf{P}_{s3}$, which is passed to the tether model to compute $\mathbf{P}_{\text{tether}}(t+1)$. The resulting tether length exceeds L_{\max} , indicating a violation. (2) The pivot shifts to p_2 , and the augmented path $\mathbf{P}_{\text{tether}}^{(0:2)} \cup \mathbf{P}_{s2}$ is evaluated, but still violates the constraint. (3) With pivot at p_1 , the augmented path $\mathbf{P}_{\text{tether}}^{(0:1)} \cup \mathbf{P}_{s1}$ yields a feasible configuration $\mathbf{P}_{\text{tether}}(t+1)$ with $L_{\text{tether}} \leq L_{\max}$. (4) The recovery path $\mathbf{P}_{\text{recovery}}$ is thus executed, consisting of \mathbf{P}_{r1} , tracing back from p_3 to p_1 , and $\mathbf{P}_{r2} = \mathbf{P}_{s1}$, leading to the waypoint $\mathbf{W}[k]$.

Algorithm 2: Entanglement-aware path planner

Input : \mathbf{W} , L_{\max} , $\mathbf{P}_{\text{tether}}(t)$, $\mathbf{p}_{\text{rov}}(t)$
Output: $\mathbf{p}_{\text{target}}$

$\text{mode} \leftarrow \text{NORMAL};$
 $\mathbf{P}_{\text{recovery}} \leftarrow \emptyset;$
 $k \leftarrow 0;$
 $L_{\text{tether}}(t) \leftarrow \text{computeLength}(\mathbf{P}_{\text{tether}}(t));$

if $\text{mode} = \text{NORMAL}$ **then**

if $L_{\text{tether}}(t) > L_{\max}$ **then**

$\text{mode} \leftarrow \text{RECOVERY};$
 $\mathbf{P}_{\text{recovery}} \leftarrow$
 $\quad \text{deEntanglementSearch}(\mathbf{P}_{\text{tether}}(t), \mathbf{W}[k]);$
 $\mathbf{p}_{\text{target}} \leftarrow \text{followPath}(\mathbf{P}_{\text{recovery}}, \mathbf{p}_{\text{rov}}(t));$

else

$\mathbf{p}_{\text{target}} \leftarrow \mathbf{W}[k];$
if $\text{reachedWaypoint}(\mathbf{p}_{\text{rov}}(t), \mathbf{W}[k])$ **then**
 $\quad k \leftarrow k + 1;$

else if $\text{mode} = \text{RECOVERY}$ **then**

$\mathbf{p}_{\text{target}} \leftarrow \text{followPath}(\mathbf{P}_{\text{recovery}}, \mathbf{p}_{\text{rov}}(t));$
if $\text{reachedEndOfPath}(\mathbf{p}_{\text{rov}}(t), \mathbf{P}_{\text{safe}})$ **then**
 $\quad \text{mode} \leftarrow \text{NORMAL};$

return $\mathbf{p}_{\text{target}};$

Algorithm 3: Disentanglement path search

Input : $\mathbf{P}_{\text{tether}}(t)$, $\mathbf{W}[k]$, L_{\max}
Output: Recovery path $\mathbf{P}_{\text{recovery}}$

$\text{found_feasible} \leftarrow \text{False};$
 $n \leftarrow \text{len}(\mathbf{P}_{\text{tether}}(t));$

for $i \leftarrow n - 1$ **downto** 0 **do**

$\mathbf{p}_{\text{pivot}} \leftarrow \mathbf{P}_{\text{tether}}(t)[i];$
 $\mathbf{P}_{r1} \leftarrow \text{reverseSegment}(i, n - 1, \mathbf{P}_{\text{tether}}(t));$
 $\mathbf{P}_{s(n-i)} \leftarrow \text{planShortestPath}(\mathbf{p}_{\text{pivot}}, \mathbf{W}[k]);$
 $\mathbf{P}_{\text{aug}} \leftarrow \text{concatenate}(\mathbf{P}_{\text{tether}}(t)[0 : i], \mathbf{P}_{s(n-i)});$
 $\mathbf{P}_{\text{tether}}(t+1) \leftarrow \text{tetherModel}(\mathbf{P}_{\text{aug}});$
 $L_{\text{tether}} \leftarrow \text{computeLength}(\mathbf{P}_{\text{tether}}(t+1));$

if $L_{\text{tether}} \leq L_{\max}$ **then**

$\mathbf{P}_{r2} \leftarrow \mathbf{P}_{s(n-i)};$
 $\text{found_feasible} \leftarrow \text{True};$
break;

if not found_feasible **then**

$\mathbf{p}_{\text{pivot}} \leftarrow \mathbf{P}_{\text{tether}}(t)[-1];$
 $\mathbf{P}_{r1} \leftarrow \emptyset;$
 $\mathbf{P}_{r2} \leftarrow \text{planShortestPath}(\mathbf{p}_{\text{pivot}}, \mathbf{W}[k]);$

$\mathbf{P}_{\text{recovery}} \leftarrow \mathbf{P}_{r1} \cup \mathbf{P}_{r2};$
return $\mathbf{P}_{\text{recovery}};$

(OMPL) library [29] is utilized to compute the shortest paths using the RRT* algorithm.

A. Simulation experimental setup

The path planner is implemented for a BlueROV2 underwater robot. An MPC approach accounts for model constraints and provides the optimal control input $\mathbf{u}^{ref} \in \mathbb{R}^4$, where $\mathbf{u}^{ref} = [F_x, F_y, F_z, M_z]^T$ represents the forces in the X , Y , and Z directions, and the moment about the Z -axis. The goal is to follow the desired reference trajectory $\mathbf{x}^{ref} \in \mathbb{R}^6$, where $\mathbf{x}^{ref} = [x_{ref}, y_{ref}, z_{ref}, \psi_{ref}]^T$ contains the reference position ($x_{ref}, y_{ref}, z_{ref}$) and the reference

yaw angle ψ_{ref} . For further details about the controller and model, the reader is referred to [30]. The entanglement-aware path planner provides \mathbf{x}^{ref} in real time, ensuring the BlueROV2 avoids obstacles while following the desired trajectory.

We perform a comparative analysis of the proposed REACT method and a baseline conventional CPP (FC-Planner [8]), which does not explicitly handle entanglement. The simulation setup uses a 1/10-scale pipe structure based on the model described in [8]. The simulated onboard camera has a 70-degree field of view. The tether constraint is implemented by specifying a maximum allowable tether length of $L_{\max} = 10\text{m}$. Note that the resulting planned trajectories are

TABLE I: Coverage performance comparison between REACT and CPP baseline showing inspection time, recovery time, total mission duration, and final environmental coverage.

Planner	Inspection time (s)	Recovery time (s)	Total time (s)	Coverage (%)
REACT	546	134	680	99.91
CPP	429	426	855	99.82

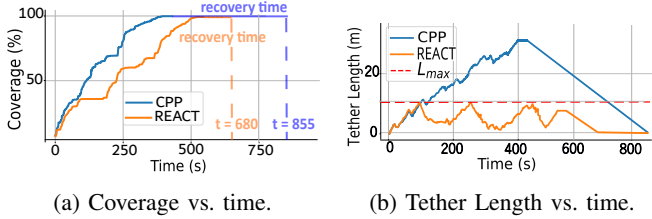


Fig. 4: Comparison of coverage and tether behavior over time.

geometrically identical to those in the full-scale environment, simply scaled down proportionally. The primary motivation for using the scaled model is to accelerate simulation runs while preserving the validity of the results.

Coverage is computed in a manner similar to [9]. At each time step, the position and orientation of the camera are used to determine which triangles in the environment mesh are visible. A triangle is marked as visible if its centroid is within the inspection range, its surface normal faces the camera, and its projection lies within the camera's field of view. Over time, the set of all uniquely observed triangles accumulates. The coverage at time t is defined as the ratio of the number of unique visible triangles up to time t to the total number of triangles in the environment.

B. Simulations results

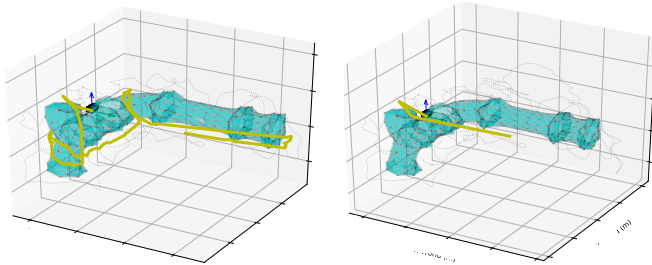


Fig. 5: 3D views of final trajectories: (a) CPP results in entangled tether path, (b) REACT yields a non-entangled tether path, reflecting effective entanglement avoidance.

TABLE II: Comparison of tether constraint compliance showing the maximum tether length reached and the total duration of tether length exceedance.

Planner	Maximum tether length (m)	Duration of length exceedance (s)
CPP	31.16	327.37
REACT	10.52	10.36

The performance metrics for both planners are summarized in Table I and Table II, while Figs. 4 and 5 visualize the performance of the planners in terms of environmental coverage, tether length behavior, and final trajectory configurations. The evaluation focuses on comparing mission efficiency, constraint compliance, and safety aspects between the entanglement-aware REACT method and the conventional CPP baseline approach.

The results present two phases: the inspection phase and the recovery phase, where the recovery time represents the estimated duration required to return to the starting position after complete inspection while disentangling the entire tether. The results highlight distinct trade-offs between the two planning strategies. As shown in Table I, the CPP method achieves a shorter inspection time (429s vs. 546s) due to its straightforward path execution without rerouting for disentanglement. However, focusing solely on inspection speed overlooks the critical aspect of tether management in constrained environments. The CPP exhibits a significantly longer total mission time (855s vs. 680s) because extensive disentanglement is required after inspection completion.

REACT demonstrates multiple instances of entanglement detection and resolution, as evidenced by the peaks in the tether length curve in Fig. 4b and the corresponding flat regions in the coverage curve in Fig. 4a, where the ROV inspection progress stops to reroute and find paths without entanglement. This reactive replanning behavior directly results in a longer inspection time, as the system prioritizes tether safety over raw speed.

In particular, the limit on the length of the tether is rarely exceeded by REACT, as shown in Table II and Fig. 4b. Conversely, the CPP method severely violates this constraint, reaching 31.16m for extended periods (327.37s), risking unrecoverable tether entanglement. The 3D trajectory visualizations in Fig. 5 further illustrate this difference, showing the entangled tether geometry resulting from CPP versus the non-entangled configuration achieved by REACT. Therefore, REACT demonstrates superior performance for safe tethered ROV inspection.

VII. REAL-WORLD EXPERIMENTS

This section presents real-world experimental results validating the proposed REACT method. The experiments were conducted at the underwater robotics facility of the German Research Center for Artificial Intelligence (DFKI), which features a 23m×19m×8m test basin equipped with a 12-camera Qualisys motion capture system for precise state estimation.

A. Real-world experimental setup

The experimental platform is a BlueROV2, configured identically to the simulation setup. The test environment consists of a pipe structure with a diameter of 0.7m and a length of 2.5m, as shown in Fig. 6. Two planning modes, identical to those evaluated in simulation, are tested. The first is REACT, which represents the full system incorporating REACT. The second is the CPP baseline without REACT.

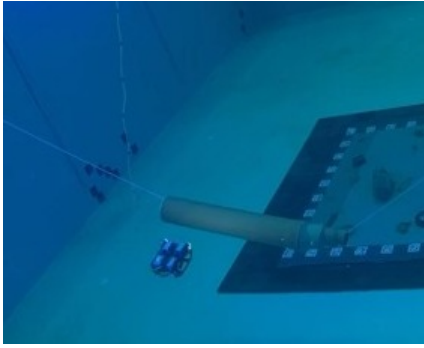


Fig. 6: Experimental setup in the DFKI underwater basin showing the BlueROV2 and the test structure. The pipe is suspended horizontally in the water using cables.

In both modes, a helical trajectory is given as a reference around the pipe.

B. Real-world experimental results

Real-world tests illustrate the clear benefits of the REACT planner compared to the baseline CPP approach. Figure 7 shows the mission trajectories for both methods. As such, the baseline CPP planner failed to complete the inspection task. At $t = 124$ s, the tether entangles the pipe structure, stopping the ROV and preventing further progress. Hence, the overall coverage achieved is only 80.9% (Table III).

The proposed REACT planner completed the full mission, achieving 95.6% coverage. The planner adapted to tether constraints throughout the mission. Unlike the simulation results, the soft tether length limit of the 8m was exceeded in real-world tests. As such, when no entanglement-free paths to the goal are available, REACT treats the length constraints as a soft limit rather than a hard limitation. However, when entanglement is detected and there is an entanglement-free path around the pipe, REACT finds a path that detangles the ROV from the structure. This capability is demonstrated at $t = 96$ s when REACT detected an imminent tether entanglement. The planner computed a new path that safely untangled the ROV from the pipe structure, allowing inspection to continue. The system only exceeded the soft tether limit when necessary for mission completion while prioritizing entanglement avoidance whenever possible.

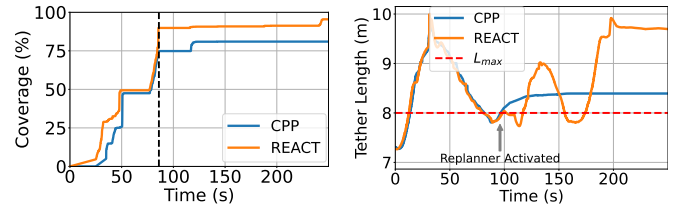
The baseline CPP planner, lacking entanglement-awareness, became permanently stuck. This demonstrates a key advantage of REACT that was not visible in the simulation study, where the physical tether forces remain unmodeled.

Although the REACT planner adds computation compared to the baseline, the maximum replanning time of 0.4822 s remained well within the onboard platform's capabilities, allowing real-time operation. This overhead, while higher than the conventional CPP approach, was low enough to enable timely adaptation to tether entanglement events.

These results demonstrate that standard planners without tether constraints fail even during relatively simple underwater 3D inspection tasks. While the baseline initially followed

TABLE III: Coverage Performance in Real-world Trials

Planner	Inspection Completion	Final Coverage (%)
REACT	Full	95.6
CPP	Failed (Entangled)	80.9



(a) Coverage vs. time for both planners. (b) Tether length vs. time for both planners.

Fig. 7: Real-world ROV trajectories. Without REACT, the mission fails due to tether entanglement. With REACT, the ROV completes the mission successfully. At $t = 96$ s, the replanner is activated, allowing REACT to disentangle the ROV and continue the inspection. In contrast, at $t = 124$ s, the ROV using the conventional CPP becomes stuck due to the entangled tether.

the planned path, it became entangled and subsequently immobilized midway through the mission. On the other hand, REACT's ability to detect and avoid entanglement through replanning enabled a successful mission completion. These findings highlight the need for entanglement-aware planning in real underwater operations.

VIII. CONCLUSION

We present REACT, a real-time, entanglement-aware path planning framework for tethered underwater vehicles that supports underwater asset inspection tasks. Through comparative simulation and real-world experiments, we demonstrate that conventional planners face tether entanglement issues, rendering incomplete missions, as they cannot account for tether constraints. In simulation, REACT shows effective tether management while maintaining full coverage, achieving a shorter total mission time (680s vs. 855s) despite longer inspection time due to its proactive entanglement avoidance that eliminates the need for extensive post-mission disentanglement. The real-world experiments confirm these findings, where the baseline CPP planner achieves only 80.9% coverage before becoming physically stuck due to tether entanglement, while REACT completes the full mission with 95.6% coverage through adaptive replanning. Additionally, REACT mitigates potential entanglement through reactive replanning, offering a more robust and reliable solution. REACT improves mission safety and integrity, making it ideal for tethered vehicle inspection scenarios where entanglement-awareness is critical.

ACKNOWLEDGMENT

This research was supported by Innovation Fund Denmark (Grant No. 2040-00032B) and EIVA a/s. The authors thank Nicolas Dahn, Dr. Leif Christensen, and Tom Slawik from

DFKI for their assistance with the experiments, and Adis Hodzic from EIVA for his technical support with the ROV control software. We also thank Dr. Louis Petit for his insights on the ropeRRT planning method and for open-sourcing his OMPL-based implementation and Dr. Olaya Álvarez-Tuñón for her valuable technical discussions.

REFERENCES

- [1] A. Amer, O. Álvarez-Tuñón, H. İ. Uğurlu, J. L. F. Sejersen, Y. Brodskiy, and E. Kayacan, “Unav-sim: A visually realistic underwater robotics simulator and synthetic data-generation framework,” in *2023 21st International Conference on Advanced Robotics (ICAR)*. IEEE, 2023, pp. 570–576.
- [2] A. Amer, D. Felsager, Y. Brodskiy, and A. Sarabakha, “Modelling of underwater vehicles using physics-informed neural networks with control,” 2025. [Online]. Available: <https://doi.org/10.48550/arXiv.2504.20019>
- [3] T. Creutz, B. Wehbe, S. Arnold, and M. Hildebrandt, “Towards robust autonomous underwater docking for long-term under-ice exploration,” in *OCEANS 2023-Limerick*. IEEE, 2023, pp. 1–8.
- [4] R. Almadhoun, T. Taha, L. Seneviratne, J. Dias, and G. Cai, “A survey on inspecting structures using robotic systems,” *International Journal of Advanced Robotic Systems*, vol. 13, no. 6, p. 1729881416663664, 2016.
- [5] T. M. Cabreira, L. B. Brisolara, and F. J. Paulo R, “Survey on coverage path planning with unmanned aerial vehicles,” *Drones*, vol. 3, no. 1, p. 4, 2019.
- [6] J. G. Hansen, M. Heiß, D. Li, M. Kozłowski, and E. Kayacan, “Vessel inspection in-the-wild: Practical planning in large-scale industrial environments,” in *2023 American Control Conference (ACC)*. IEEE, 2023, pp. 812–817.
- [7] A. Bircher, K. Alexis, M. Burri, P. Oettershagen, S. Omari, T. Mantel, and R. Siegwart, “Structural inspection path planning via iterative viewpoint resampling with application to aerial robotics,” in *2015 IEEE International Conference on Robotics and Automation (ICRA)*. IEEE, 2015, pp. 6423–6430.
- [8] C. Feng, H. Li, M. Zhang, X. Chen, B. Zhou, and S. Shen, “Fc-planner: A skeleton-guided planning framework for fast aerial coverage of complex 3d scenes,” in *2024 IEEE International Conference on Robotics and Automation (ICRA)*. IEEE, 2024, pp. 8686–8692.
- [9] A. Amer, M. Mehndiratta, J. le Fevre Sejersen, H. X. Pham, and E. Kayacan, “Visual tracking nonlinear model predictive control method for autonomous wind turbine inspection,” in *2023 21st International Conference on Advanced Robotics (ICAR)*. IEEE, 2023, pp. 431–438.
- [10] T. Dang, M. Tranzatto, S. Khattak, F. Mascari, K. Alexis, and M. Hutter, “Graph-based subterranean exploration path planning using aerial and legged robots,” *Journal of Field Robotics*, vol. 37, no. 8, pp. 1363–1388, 2020.
- [11] R. P. De Figueiredo, J. le Fevre Sejersen, J. G. Hansen, M. Brandão, and E. Kayacan, “Real-time volumetric-semantic exploration and mapping: An uncertainty-aware approach,” in *2021 IEEE/RSJ International Conference on Intelligent Robots and Systems (IROS)*. IEEE, 2021, pp. 9064–9070.
- [12] G. Battocletti, D. Boskos, D. Toliae, I. Palunko, and B. De Schutter, “Entanglement definitions for tethered robots: Exploration and analysis,” *IEEE access*, 2024.
- [13] S. McCammon and G. A. Hollinger, “Planning and executing optimal non-entangling paths for tethered underwater vehicles,” in *2017 IEEE International Conference on Robotics and Automation (ICRA)*. IEEE, 2017, pp. 3040–3046.
- [14] L. Mechsy, M. Dias, W. Pragithmukar, and A. Kulasekera, “A novel offline coverage path planning algorithm for a tethered robot,” in *2017 17th International Conference on Control, Automation and Systems (ICCAS)*. IEEE, 2017, pp. 218–223.
- [15] X. Peng, F. Schwarzentruer, O. Simonin, and C. Solnon, “Spanning-tree based coverage for a tethered robot,” *IEEE Robotics and Automation Letters*, 2025.
- [16] S. Kim, S. Bhattacharya, and V. Kumar, “Path planning for a tethered mobile robot,” in *2014 IEEE International Conference on Robotics and Automation (ICRA)*. IEEE, 2014, pp. 1132–1139.
- [17] V. S. Chipade, R. Kumar, and S. Z. Yong, “Withy a*: Winding-constrained motion planning for tethered robot using hybrid a,” in *2024 IEEE International Conference on Robotics and Automation (ICRA)*. IEEE, 2024, pp. 8771–8777.
- [18] S. Hert and V. Lumelsky, “The ties that bind: Motion planning for multiple tethered robots,” *Robotics and autonomous systems*, vol. 17, no. 3, pp. 187–215, 1996.
- [19] X. Zhang and Q.-C. Pham, “Planning coordinated motions for tethered planar mobile robots,” *Robotics and Autonomous Systems*, vol. 118, pp. 189–203, 2019.
- [20] M. Cao, K. Cao, S. Yuan, T.-M. Nguyen, and L. Xie, “Neptune: nonentangling trajectory planning for multiple tethered unmanned vehicles,” *IEEE Transactions on Robotics*, vol. 39, no. 4, pp. 2786–2804, 2023.
- [21] S. Bhattacharya, M. Likhachev, and V. Kumar, “Topological constraints in search-based robot path planning,” *Autonomous Robots*, vol. 33, pp. 273–290, 2012.
- [22] S. Martinez-Rozas, D. Alejo, F. Caballero, and L. Merino, “Optimization-based trajectory planning for tethered aerial robots,” in *2021 IEEE International Conference on Robotics and Automation (ICRA)*. IEEE, 2021, pp. 362–368.
- [23] L. Petit and A. L. Desbiens, “Tape: Tether-aware path planning for autonomous exploration of unknown 3d cavities using a tangle-compatible tethered aerial robot,” *IEEE Robotics and Automation Letters*, vol. 7, no. 4, pp. 10550–10557, 2022.
- [24] S. Hert and V. Lumelsky, “Motion planning in r/sup 3/for multiple tethered robots,” *IEEE transactions on robotics and automation*, vol. 15, no. 4, pp. 623–639, 1999.
- [25] A. Patil, M. Park, and J. Bae, “Coordinating tethered autonomous underwater vehicles towards entanglement-free navigation,” *Robotics*, vol. 12, no. 3, p. 85, 2023.
- [26] M. Cao, K. Cao, S. Yuan, K. Liu, Y. L. Wong, and L. Xie, “Path planning for multiple tethered robots using topological braids,” *arXiv preprint arXiv:2305.00271*, 2023.
- [27] A. Millane, H. Oleynikova, E. Wirbel, R. Steiner, V. Ramasamy, D. Tingdahl, and R. Siegwart, “nvblox: Gpu-accelerated incremental signed distance field mapping,” in *2024 IEEE International Conference on Robotics and Automation (ICRA)*. IEEE, 2024, pp. 2698–2705.
- [28] L. Petit and A. L. Desbiens, “Rrt-rope: A deterministic shortening approach for fast near-optimal path planning in large-scale uncluttered 3d environments,” in *2021 IEEE International Conference on Systems, Man, and Cybernetics (SMC)*. IEEE, 2021, pp. 1111–1118.
- [29] I. A. Sucan, M. Moll, and L. E. Kavraki, “The open motion planning library,” *IEEE Robotics & Automation Magazine*, vol. 19, no. 4, pp. 72–82, 2012.
- [30] A. Amer, M. Mehndiratta, Y. Brodskiy, and E. Kayacan, “Empowering autonomous underwater vehicles using learning-based model predictive control with dynamic forgetting gaussian processes,” *IEEE Transactions on Control Systems Technology*, 2025.